2022

Introducing an H113A mutation into Atg10 Y73Q to reduce autophagic activity and understand the effect of Atg on autophagosome size and number

Konrad L. Lautenschlager

Introducing an H113A mutation into Atg10 Y73Q to reduce autophagic activity and understand the effect of Atg on autophagosome size and number

Abstract

Autophagy is an essential recycling process that occurs within eukaryotic cells, however, the individual functions of the current thirty-two known autophagic proteins are not yet entirely understood. At this time, it is known that the autophagic protein Atg7 works upstream of both Atg3 and Atg10. Atg3 is affected by Atg7 and allows for the attachment of Atg8 and the lipid PE which is part of the autophagosome membrane. The Atg10 pathway is also affected by Atg7 but attaches Atg12 to Atg5 which upregulates the function of Atg3 and ultimately Atg8 lipidation. These protein interactions are necessary for forming autophagosomes, large double membrane vesicles that carry cytoplasmic cargo to the lysosome or vacuole by way of autophagy. Previous research has documented that Atg7 affects both the size and the number of autophagosomes formed, while Atg8 affects primarily the size of the autophagosomes. It is our hypothesis that some step in either pathway might be affecting the number of autophagosomes or possibly both size and number like Atg7. Our lab is currently focusing on the Atg10 pathway, and therefore creating Atg10 mutants that show a partial loss of autophagic activity; comparing these to the wild type will allow us to analyze the differences in autophagosome size and number that result from the reduction of the Atg10 function. We created a double mutant (H131A and Y73Q) in Atg10 and used western blots of pre-Ape1 and mature-Ape1, a specific autophagic cargo, along with the Pho8Δ60 assay of bulk autophagy, to determine if it retains ~30-40% of autophagic activity, suitable for further testing and eventually TEM.

Degree Type

Open Access Senior Honors Thesis

Department or School

Neuroscience

First Advisor

Steven K. Backues, Ph.D.

Second Advisor

Hedeel Evans, Ph.D.

Third Advisor

Deborah Heyl-Clegg, Ph.D.

Subject Categories

Chemistry | Neuroscience and Neurobiology

INTRODUCING AN H131A MUTATION INTO ATG10 Y73Q TO REDUCE AUTOPHAGIC ACTIVITY AND UNDERSTAND THE EFFECT OF ATG10 ON AUTOPHAGOSOME SIZE AND NUMBER

By

Konrad L. Lautenschlager

A Senior Project Submitted to the

Eastern Michigan University

Honors College

In Partial Fulfillment of the Requirements for Graduation

with Departmental Honors in Neuroscience

and with Highest Honors

Approved in Ypsilanti, MI on December 20, 2022

Project Advisor:	Steven K. Backues, Ph.D.
Departmental Honors Advisor:	Hedeel Evans, Ph.D.
Department Head/School Director:	Deborah Heyl-Clegg, Ph.D.
Dean of The Honors College:	Ann R. Eisenberg, Ph.D.

Table of Contents

SECTION 1: ABSTRACT

Autophagy is an essential recycling process that occurs within eukaryotic cells, however, the individual functions of the current thirty-two known autophagic proteins are not yet entirely understood. At this time, it is known that the autophagic protein Atg7 works upstream of both Atg3 and Atg10. Atg3 is affected by Atg7 and allows for the attachment of Atg8 and the lipid PE which is part of the autophagosome membrane. The Atg10 pathway is also affected by Atg7 but attaches Atg12 to Atg5 which upregulates the function of Atg3 and ultimately Atg8 lipidation. These protein interactions are necessary for forming autophagosomes, large double membrane vesicles that carry cytoplasmic cargo to the lysosome or vacuole by way of autophagy. Previous research has documented that Atg7 affects both the size and the number of autophagosomes formed, while Atg8 affects primarily the size of the autophagosomes. It is our hypothesis that some step in either pathway might be affecting the number of autophagosomes or possibly both size and number like Atg7. Our lab is currently focusing on the Atg10 pathway, and therefore creating Atg10 mutants that show a partial loss of autophagic activity; comparing these to the wild type will allow us to analyze the differences in autophagosome size and number that result from the reduction of the Atg10 function. We created a double mutant (H131A and Y73Q) in

Atg10 and used western blots of pre-Ape1 and mature-Ape1, a specific autophagic cargo, along with the Pho8Δ60 assay of bulk autophagy, to determine if it retains ~30-40% of autophagic activity, suitable for further testing and eventually TEM.

SECTION 2: INTRODUCTION

The word "autophagy" comes from the Greek language and translates literally to "self-eating", which is exactly the function that this process carries out within the cell (Choi *et al.* 2013). More specifically, this process takes place within eukaryotic cells, including plants, animals, and fungi. One such eukaryotic cell is yeast, which we use in our lab to perform experiments, as they contain the autophagic machinery required for this process (Reggiori and Klionsky 2002). We understand the vast importance of this process because the lack of autophagy has been found to bring about many illnesses including those that are neurodegenerative in nature, such as Parkinson's and Alzheimer's, as well as cancer; additionally, the lack of autophagy also increases the ability of pathogens to disrupt the cell's homeostasis (Choi *et al.* 2013). It has also been documented that as a cell ages the levels of autophagy decrease, resulting in aging effects. Our research is focused primarily on finding the steps required to do this "self-eating".

Autophagy includes the finding of a target (damaged materials/ pathogens) in the cytoplasm that will be broken down, the making of a double-membrane vesicle that encapsulates that material, and then bringing the formed autophagosome back to either a lysosome or vacuole depending on if the cell is animal or plant/fungi derived (Figure 1). Vacuoles are found in plants and fungi, whereas lysosomes are found in animal cells, however, both serve a similar function in that they metabolize, degrade, and recycle the contents of the autophagosome when it arrives

at either (Choi *et al.* 2013). These components that are broken down are recycled in a way that allows them to be reused and maintain a homeostatic environment within the cell.

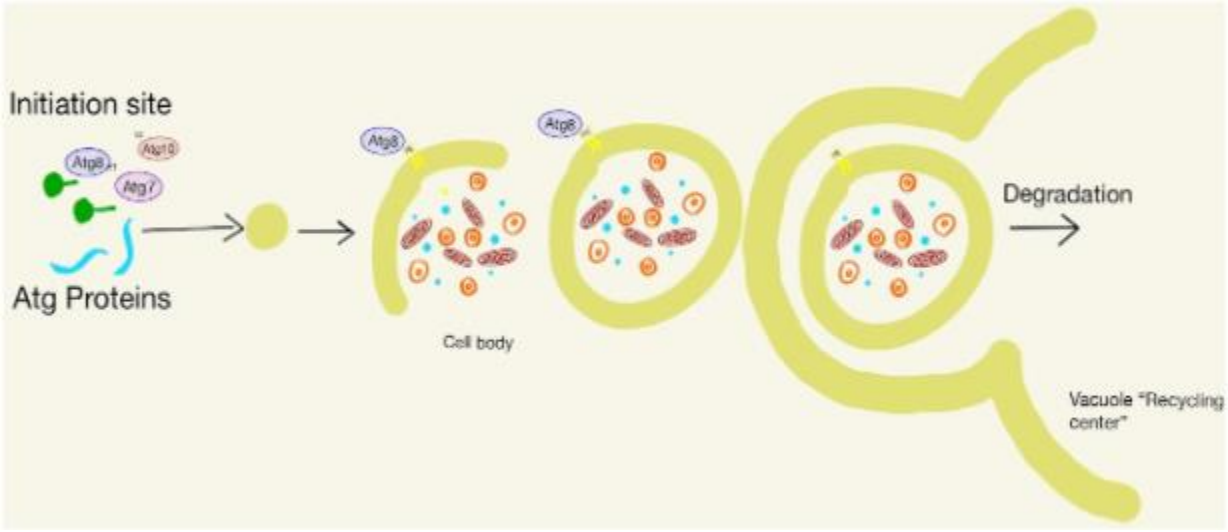

Figure 1: Atg8 and other autophagic proteins forming the autophagosome and entering the lysosome or vacuole. Image credit: Nadia Silvia, Backues Lab (made in GoodNotes)

There are two types of autophagy: selective and non-selective. Non-selective autophagy occurs in response to starvation: when the cell is low on nutrients, autophagy occurs and cargo within the cytoplasm is "randomly" broken down and its components recycled or disposed of (Figure 2). In selective autophagy a very specific part or component of the cell is removed. Sometimes this includes the breakdown of a certain organelle within the cell such as the mitochondria (mitophagy), a pathogen (xenophagy), or a protein aggregate (aggrephagy) (Reggiori and Klionsky 2013, Choi *et al.* 2013). Another selective pathway is the cvt pathway (cytoplasm-to-vacuole targeting) which is specific to yeast and includes the transport of hydrolases to the vacuole in yeast (Yamasaki and Noda 2017) (Figure 2).

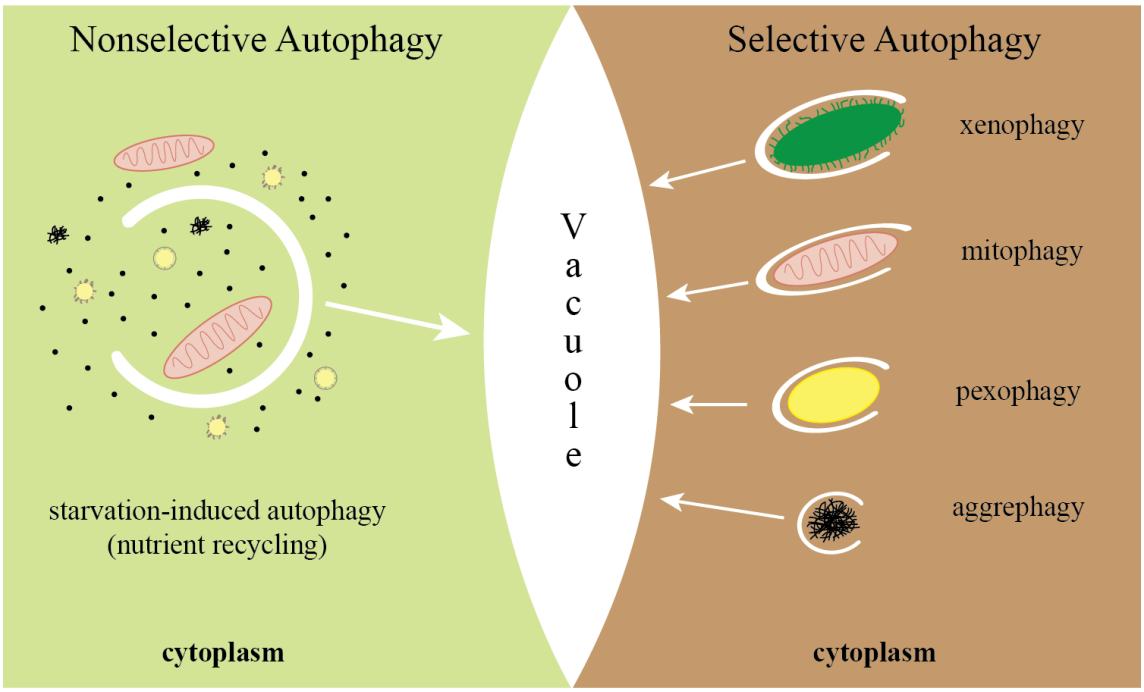

Figure 2: Nonselective autophagy is induced by starvation, while selective autophagy targets specific cargo within the cell in response to particular cellular events. Image credit: Dr. Steven K. Backues, PhD (made in Adobe Illustrator)

A cascade of about thirty autophagy proteins, which are abbreviated with "Atg", interact with one another to collect cargo, whether selective or non-selective, and bring it to the vacuole for degradation in yeast cells (Xie and Klionsky 2007, Matoba and Noda 2021). Within this project the primary focus is Atg10, its associated Atg proteins, and how they affect autophagy in yeast during starvation conditions. *Saccharomyces cerevisiae*, baker's yeast, is the species used in our lab as it is convenient to use in the lab setting, while still being well conserved to mammalian cells (Reggiori & Klionsky, 2013).

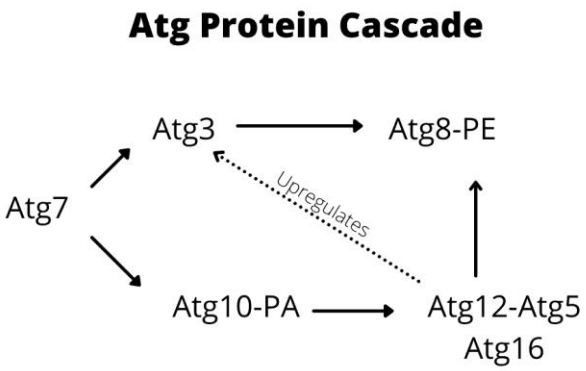

Figure 3: Autophagic cascade starting with Atg7, which is known to affect both autophagosome size and number. The end-product is Atg8-PE; Atg8 has been determined to affect the size of the autophagosome constructed. We will look at Atg10 and its effect on the conjugation of Atg12 to Atg5 and ultimately the formation of Atg8-PE and the autophagosome. Image credit: Konrad Lautenschlager, Backues Lab (made in Google Slides)

Atg7 is found at the start of the cascade seen in Figure 3 and is responsible for initiating two separate pathways that lead to other Atg protein interactions and ultimately Atg8 lipidation with PE (phosphatidylethanolamine), a lipid within the plasma membrane of the autophagosome (Cawthon et al. 2018). In experimental data collected by Cawthon *et al.*, insufficient levels of Atg7 resulted in a reduction in both size and number of the autophagosome, suggesting Atg7 has an effect on both size and number (2018). Their lab also discovered that Atg8 and its interaction with PE was affecting primarily the size of the autophagosome. This suggests that an interaction in the pathways leading to Atg8 lipidation from Atg7 may be affecting the number or both size and number of the autophagosomes (Cawthon et al. 2018). As a result of these findings, we hypothesize that interactions in the Atg3 and Atg10 pathways, particularly that of the Atg12-5 conjugation in the Atg10 pathway, which upregulates Atg3, has an effect on the size and number of the autophagosome (Figure 3).

In order to understand Atg10's function to greater extent and how it helps to conjugate the Atg12-Atg5-HA-Atg16 complex, we will be creating potential atg10 mutants that show a partial loss of function, preferably with 60-70% less activity than the wild type, which we can then compare to our wild type Atg10 using techniques that measure autophagic activity. It is important that these mutations cause a reduction in function, not a complete loss, because we already know from atg10Δ mutants that without the *ATG10* gene autophagic function is almost completely eradicated. The Atg10 mutations we made can be thought of as the independent variable, and the level of autophagic activity measured can be thought of as the dependent variable. We are altering one part of the cascade and hoping to discover how that change affects the rest of the autophagic cascade.

Our lab initially tested two single mutants: Atg10 H131A and Atg10 Y73Q. These were originally chosen because they looked promising based on empirical data reported by Yamaguchi et al. (2012). While these did show a slight reduction in autophagic activity in previous tests performed in our lab (western blot and ALP assay), the reduction was found not to be significant enough to consider it effective for comparison to the wild type (Silvia 2022). Different mutations or additional mutations needed to be made in order to further decrease autophagic activity to a testable level; preferably we would like to have mutants with autophagic activity at 30-40% and 60-70% that of the wild type.

As a result of our previous mutants having little or no reduction in autophagic activity, the next step was to make a mutant with a double mutation. Because the single mutation mutant already existed, introducing an additional mutation to these would result in a double mutant. This was done by integrating the H131A mutation into the already existing pRS406-Atg10-Y73Q mutant.

By quantifying the effects of the autophagic proteins, like Atg10, on the size and number of autophagosomes, their function in the process can be further evaluated and understood. The size and number of these autophagosomes is relevant because it helps us understand the manner in which they are formed in response to the interaction of the Atg proteins and the uptake of cargo within the cell (Cawthon, *et al* 2018). With a better understanding of the autophagic processes, research related to cellular upkeep and maintenance will become more effective, which in turn would allow for its application in the realm of medicine and human health.

SECTION 3: MATERIALS AND METHODS

Atg10 Y73Q and H131A Mutants

These mutations were created by site-directed mutagenesis. Primers were purchased from Integrated DNA Technologies. We used primers 488 and 489 (Table 3) to introduce the H131A mutation to the existing pRS406 Atg10-PA Y73Q template (CAT→GCA). The PCR "ingredients" (Table 1) were mixed in PCR tubes and placed in a BioRad MyCyclerTM thermal cycler where the denaturation, annealing, and extension of the DNA takes place (Table 2).

Table 1: 100µL PCR Reaction Materials

ddH_2O (PCR bench)	66µL
Buffer	20µL
dNTP 10mM	2µL
F primer SKB 488	5µL
R primer SKB 489	5µL
pRS406 Atg10-PA Y73Q template	1µL
New England Biolabs Phusion HF polymerase	1µL

(NEB)	

Table 2: PCR Reaction Times and Temperatures (Cycles 35x from Denaturation to Extension)

Initial Denaturation	9℃	30s
Denaturation	98℃	10s
Annealing	70℃ (488+489)	20s
Extension	72℃	3:15s 45s (based on Kb)
Final Extension	72℃	5 min
Hold	16℃	infinite

Table 3: Primers used

SKB 20	M13 R	M13 reverse primer (pDONR221)	CAGGAAACAGCTATGAC
SKB 432	PA +100 R	Sequencing primer (reverse) starting 100bp into the PA-tag	CTTTGGATGAAGGCGTTTCG
SKB 488	Atg10 mut H131A F	Mutates H131A, CAT to GCA. Use with SKB489	TATTCTTTCGCACCATGCGATACAT CATGTATAGTAGGTGA
SKB 489	Atg10 mut H131A R	Mutates H131A, CAT to GCA. Use with SKB488	TATCGCATGGTGCGAAAGAATACC AAACGCTACCT

Agarose Gel Electrophoresis

50 mL 1.0% Agarose gels were used for electrophoresis and were prepared using 50 mL 1x TAE, 0.5 grams agarose, and 1.5µL Gel Red. 2µL of 5x loading dye was added to 5µL of the PCR products before loading them into the gel to ensure that they are visible on the physical gel and that they sink to the bottom of the well. 7µL of each sample and 8µL of the DNA ladder was loaded. The gel was run for approximately 45 minutes at 100V (until the dye front reaches the end of the gel), using a Horizontal Electrophoresis System from Fisher Biotech and an EC135 power supply from E-C Apparatus Corporation.

PCR Purification

1μL of Dpn1, a restriction enzyme which destroys the template remaining in the PCR to reduce background, was added to the successful PCR product and incubated at 37℃. The product was then purified according to the protocol in the SpinSmart DNA PCR Purification and Gel Extraction Kit by Denville Scientific Inc.

In-Fusion

The In-Fusion reaction recirculates and connects the homologous ends of the linear PCR product to make a plasmid; this was done using the In-Fusion EcoDry cloning system (Takara Bio).

***E. coli* Transformation**

Approximately 0.5-1.0 μL of the plasmid created during the In-Fusion reaction was added to competent cells and incubated on ice for 30 minutes, then heat shocked for 42 seconds at 42℃. The samples were then incubated for additional two minutes on ice, before 1 mL SOB (Super Optimal Broth: nutrient-rich bacterial growth medium) was added and incubated for an hour at 37℃. 100 μL of this product was plated on carbenicillin selective plate for a 10% dilution. The plates were incubated overnight at 37℃.

Plasmid Mini-Prep and Sequencing

Cultures were grown up from eight independent *E. coli* clones transformed with the Atg10 Y73Q H131A In-Fusion reaction mix. We followed the protocol for the PureLink Invitrogen Quick Plasmid Miniprep Kit by Thermo Fischer Scientific to purify the eight plasmid clones and sent them out to Eton BioLabs for sequencing.

The primers used were SKB432, which starts 100 bp into the PA tag of Atg10, and SKB20, which starts at the M13 region just downstream of the terminator sequence. Both primers read reverse and yielded approximately 1000bp of usable sequence, allowing us to cover

the entirety of the Atg10 gene, as well as the promoter and PA tag sequences. The sequence was analyzed using *A Plasmid Editor*, a DNA alignment software (Davis and Jorgensen 2022).

Yeast Transformation of pRS406 Atg10-PA H131A Y73Q

We followed the yeast transformation protocol outlined by Gietz and Schiestl (2007). The pRS406 Atg10-PA H131A Y73Q Clones 5 + 6 plasmids that had been purified by DNA miniprep and verified were linearized by the addition of restriction enzyme Stu1, and then integrated into atg10Δ yeast cells. Cultures were grown overnight in YPD, diluted to OD 0.2 in 5 mL YPD and then grown to log phase, about 0.8-1.0 OD (approximately 4 hours). The cells were then centrifuged, washed, and placed into a 1.5 ml centrifuge tube where the supernatant was removed. The pellet was resuspended in 240 µL 50% v/v PEG 3350, 36 µL 1M LiAc,10 µL 10mg/mL single stranded carrier DNA (boiled and cooled), 10 µL DNA, and 64 µL H_2O. This mixture was vortexed and incubated for 30 minutes at 42°C. It was then pelleted and the supernatant was removed. The pellet was resuspended in 1 mL water, plated on SMD-ura plates, and incubated at 30°C for 2-3 days.

Harvesting Samples for Western Blotting and the ALP Assay

1) A 3 mL culture of each desired strain was grown overnight; the following morning these were split to inoculate two 7 mL cultures to 0.2 OD. These were grown up to ~1.0 OD. In order to induce autophagy, we starved one set of samples for 3 hours; this was done by centrifuging one set of samples, decanting the supernatant, washing each pellet with 7 mL water, and resuspending in 7 mL SD-N. Then they were grown at 30°C, 300 RPM for 3 hours.
2) During this time the other set of samples (0 hour samples) were harvested. 250 µL were added to cuvettes in duplicate for each sample which were then diluted to 1 mL for OD

measurement required for WB samples. 1 mL of each culture was centrifuged and decanted and incubated in ice cold 10% TCA for 20 minutes. Samples were then pelleted for 5 minutes in the 4℃ cold room. The 10% TCA was then carefully removed via pipetting and the pellet was resuspended in 1 mL ice cold acetone and pelleted again for 5 minutes in the 4℃ room. The acetone was then also removed and the pellet was allowed to dry under the fume hood, then they were stored in a -20C freezer.

3) The remainder of the culture was centrifuged at 2000g for 2 minutes, decanted, resuspended in 1 ml of water and transferred to a 1.5 mL centrifuge tube where it was again centrifuged (13,000g for 1 min), decanted, and then stored at -20°C until the ALP assay was ready to be completed.

Steps 2 and 3 were repeated again for the 3 hour starved samples.

Western Blotting

The pellet from the TCA precipitated samples was resuspended with 1x SSB+250mM Tris, pH6.8 to 0.02 OD per µl. 25 µL glass beads were added and the samples were vortexed in the Disruptor Genie in the 4℃ cold room. The samples were placed in the heating block for 5 minutes at 95°C, centrifuged for 5 minutes at 13,000g and then 10 µL of supernatant was loaded into a 10% SDS-PAGE gel. BLUEstain™ 2 Protein ladder, 5-245 kDa (Gold Biotechnology) was used as our protein ladder. The gel was run in an SDS-PAGE running buffer at 120V for approximately 1 hour or until the dye front visibly reached the bottom of the gel.

Once the gel electrophoresis was complete, the transfer was set up using a hydrophobic PVDF Immobilon®-P Membrane (Millipore) which was first equilibrated by immersion in 95% v/v ethanol for ~10-15s, Milli-Q® water for 1-2 minutes, and Towbin transfer buffer (15mM Tris, 192 mM glycine pH 8.3, 10% v/v 95% EtOH) for >5 min. The transfer was run for 1 hour

at 120V with an ice pack and prechilled Towbin transfer buffer. Following the transfer, the membrane was submerged in Ponceau S stain which allows us to see bands on the membrane and cut at the appropriate sizes.

The Pgk1 bands were generally visible around 45 kDa, while the PAP band was found around 33.5 kDa. The cut was made just above the 3rd blue marker down between the orange and green bands on the BLUEstain™ 2 Protein ladder, which is around 37 kDa. The Pgk1 portion of the blot was blocked in 1:10,000 PGK1 primary antibody overnight in the 4°C room on a shaker. (All antibody dilutions were made in 4% w/v nonfat dry milk in TBST). The PAP does not have a primary and was therefore blocked with 4% w/v nonfat dry milk in TBST overnight in the 4°C room. After the overnight blocks, the blots were washed four times with TBST for 5 minutes on the shaker. The Pgk1 was then put on 1:5000 α-mouse secondary antibody for one hour on a shaker at room temperature. The PAP blot was put on its primary antibody; 1:500 PAP, also for one hour at room temperature.

The Ape1 blot was cut at 75 kDa, just above the orange band because Ape1 is known to be found below. It was put on 1:5,000 rabbit-α-Ape1 for the primary antibody overnight at 4°C and then on 1:5,000 goat-α-rabbit for one hour at room temperature.

After the secondary antibody incubation had been completed the membranes were washed four times for 5 minutes with TBST (1X Tris-Buffered Saline, 0.1% Tween) on a shaker. One mL of Immobilon Crescendo Western HRP substrate Millipore reagent was pipetted onto the membranes and let sit for ~1 minute. The liquid was then gently "dabbed" off and the membranes were imaged with the BioRad Chemidoc XRS+ system which detects the light produced when the HRP (Horseradish Peroxidase) chromagen is oxidized.

The images gathered were analyzed with ImageJ by Fiji. The Ape1 quantification was made by dividing the measured mApe1 by the total (preApe1 + mApe1).

ALP Assay (Pho8Δ60)

In addition to the Ape1 western blot and quantification, an ALP assay was performed to measure the overall defect in autophagic activity. WLY176 (Table 4) is a Pho8Δ60 strain and was used for this procedure (Noda and Klionsky 2008).

1) Lysis: We use the ALP samples previously collected in the combined protocol. 500 µL of ice cold lysis buffer (20 mM PIPES KOH pH 6.8, 50 mM KCl, 100 mM KOac, 10 mM $MgSO_4$, 10 µM $ZnSO_4$, 0.5% TX-100, 200 mL H_2O) and ~50 of glass beads were added and vortexed for ten minutes in the Disruptor Genie in the 4°C cold room. PMSF was added to 1 mM (from a 100 mM stock in 100% ethanol) to the lysis buffer just before use. They were then centrifuged for five minutes at 16000 g in the cold room.
2) ALP Reaction; 100 µL of the supernatant from each lysis reaction was added to a 1.7 µL centrifuge tube, additionally we made one blank sample with 100 µL lysis buffer. 400 µL prewarmed (37°C) reaction buffer (250 mM Tris-HCl pH 8.5, 10 mM KOac, 10 uM $ZnSO_4$, 0.4% TX-100, 200 mls H_2O) was added to each tube of lysate. We added PnPP powder (p-Nitrophenyl Phosphate, Disodium Salt) to the reaction buffer to bring it to 1.68 mM just before use. The reaction was incubated for 20-30 minutes at 30°C until a color change (yellow) was observed. At this point 500 µL stop solution (1 M glycine-NaOH, pH 11) was added, the vials were centrifuged for 2 minutes at 13000 g, and the absorbance was read at 420 nm on a Genesys 30 Vis Spectrophotometer (ThermoFisher).

3) BCA Protein Assay: We used the Pierce™ BCA Protein Assay Kit from Thermo Scientific to measure the protein concentration in the lysate using a BioTek Synergy 2 Plate Reader.
4) Data Analysis: The blank was subtracted from all measurements and the adjusted 420 nm absorbances were divided by the BCA Protein Assay 562 nm absorbances. The result is a percent of wild type activity; that is, if the wild type is standardized to 100%, the samples will have a certain relative percent of autophagic activity.

Throughout western blotting and ALP assays, *atg10Δ* was used as a negative control, and *ATG10-PA* was used as a positive control. These were originally prepared in *Saccharomyces cerevisiae* by previous students in the Backues lab (Silvia 2022).

Table 4: Strains used

Name	Genotype	Source
SKB422	WLY176 (*pho13*Δ *pho8*Δ*60*)	Kanki *et al.* 2009
SKB1008	WLY176 *atg10Δ::Kan* clone 1	Silvia 2022
SKB1028	SKB1008 *ATG10-PA(2)*	Silvia 2022
SKB1029	SKB1008 *ATG10-PA(4)*	Silvia 2022
SKB1030	SKB1008 *ATG10-PA* Y73Q(1)	Silvia 2022
SKB1031	SKB1008 *ATG10-PA Y73Q(2)*	Silvia 2022
SKB1032	SKB1008 *ATG10-PA H131A(2)*	Silvia 2022
SKB1033	SKB1008 *ATG10-PA H131A(4)*	Silvia 2022

(*E. coli*)	DH5α	

SECTION 4: RESULTS

As a result of the previous Atg10 single mutants having little or no reduction in autophagic activity, we decided the next step would be to make a mutant with a double mutation, so that the effects on size and number of autophagosomes formed would be more apparent. Because we already had mutants with one mutation we introduced an additional mutation to those. This was done by integrating the H131A mutation into the already existing pRS406-Atg10-Y73Q mutant.

A PCR reaction was performed with primers that mutated the CAT (histidine) nucleotides to GCA (alanine). In order to verify the PCR product, we performed agarose gel electrophoresis; the intensity of the band was used to estimate the amount of product of a given molecular weight relative to a DNA ladder, so this allowed for the verification of the copied sequence. For this PCR, a band at approximately 6.5 kB was seen, as expected.

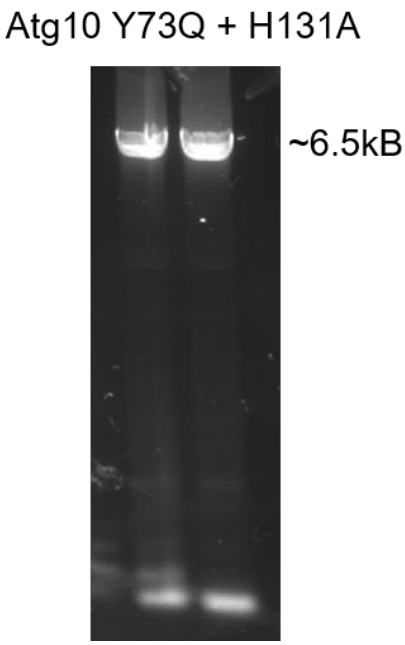

Figure 3: The PCR product pRS406 Atg10-PA Y73Q H131A was verified by gel electrophoresis prior to In-Fusion and transformation into *E. coli.* The band was close to 6.5kB, as expected.

The now doubly mutated PCR product was still linear but had complementary ends. However, for the plasmid to be properly integrated during the transformation it needed to be circular. At this point In-fusion Cloning Technology (Takara) was used to remove the complementary strands of DNA from one another at the ends of the linear PCR product and then bind the homologous ends of each with themselves resulting in a circular plasmid ready for transformation into *E. coli* (DH5α). We grew cultures from colonies resulting from this transformation and then the plasmids were then isolated, purified, and prepared for sequencing by Eton Biolabs.

Of the eight sequenced clones, the alignment of pRS406 Atg10-PA Y73Q H131A Clones 5 and 6 was best. Base pairs from 3280 → 4145 within the prs406 Atg10-PA Y73Q plasmid template aligned well with the Atg10-PA Y73Q H131A and the respective mutations were accurate, with the newly inducted H131A mutation present at base pairs 391→393 from the start of the Atg10 gene, which are base pairs 3431→3433 of the plasmid (Figure 4). Note that there was a mismatch mutation at base pair 3845 in both clones, which is located within the PA tag, however, this has been seen before and it does not affect function.

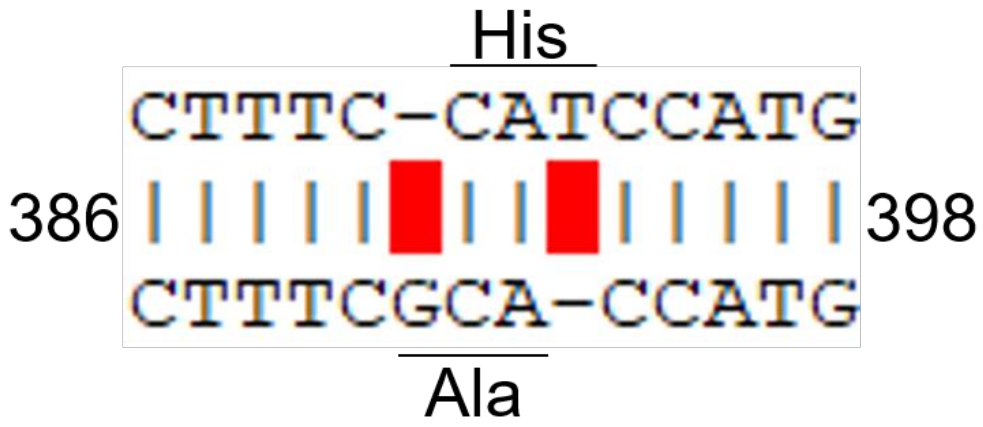

Figure 4: Alignment Sequence of prs406 Atg10-PA Y73Q plasmid template against prs406 Atg10-PA H131A Y73Q Clone. This alignment allowed for the verification of the H131A mutation at base pairs 391→393. The sequence was read using a DNA alignment software, *A Plasmid Editor* (Davis and Jorgensen 2022). The base pair numbers show the location in relation to the start of the *ATG10* gene; 386 corresponds to 3426 in the prs406 Atg10-PA Y73Q plasmid and 398 corresponds to 3438. The top strand in this alignment is the original unmutated reference sequence while the bottom strand is the sequencing result from the mutated plasmid.

After the clone sequences were verified we transformed pRS406 Atg10-PA Y73Q H131A into yeast so that we could test its function. Once the plasmid was in yeast, cultures were grown up and the samples for western blotting and an ALP assay were prepared, both of which allow for the analysis of autophagic activity.

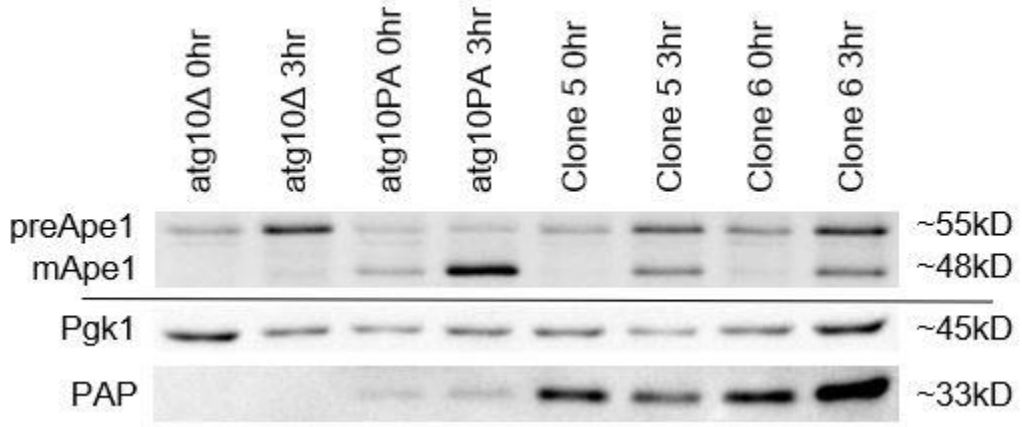

A.

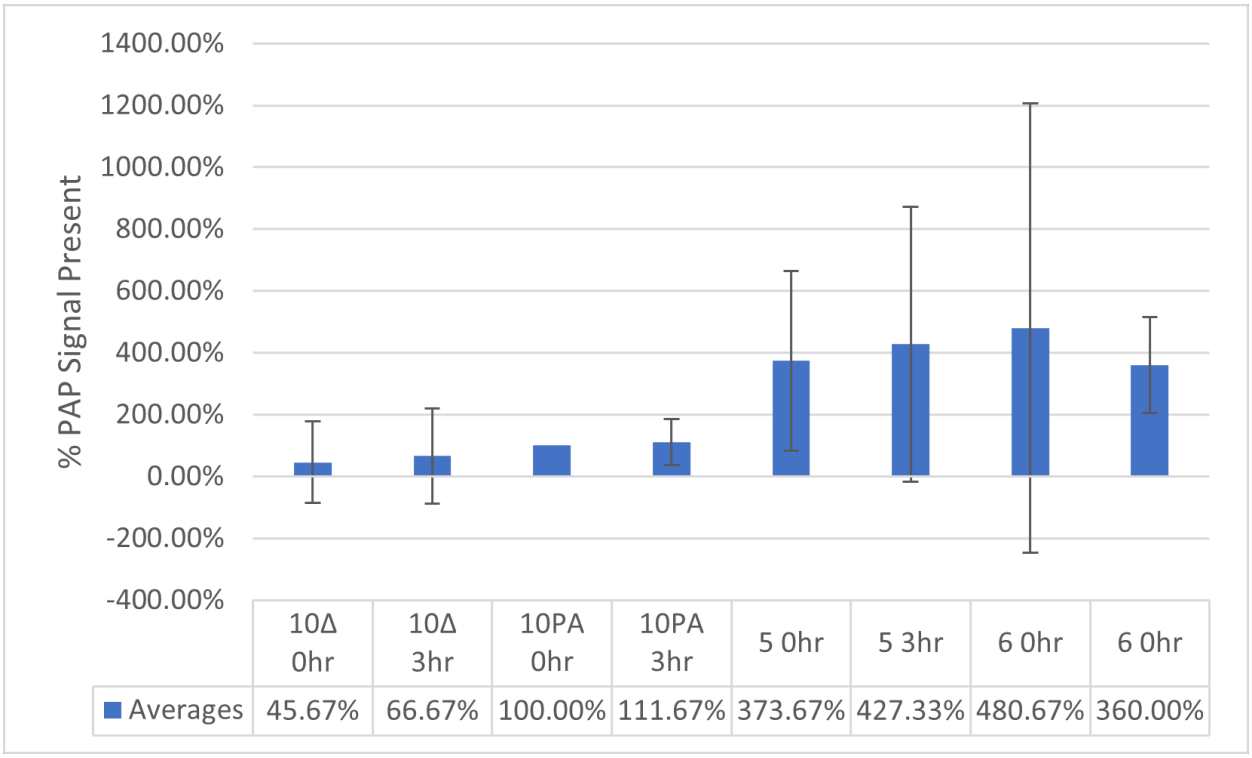

B.

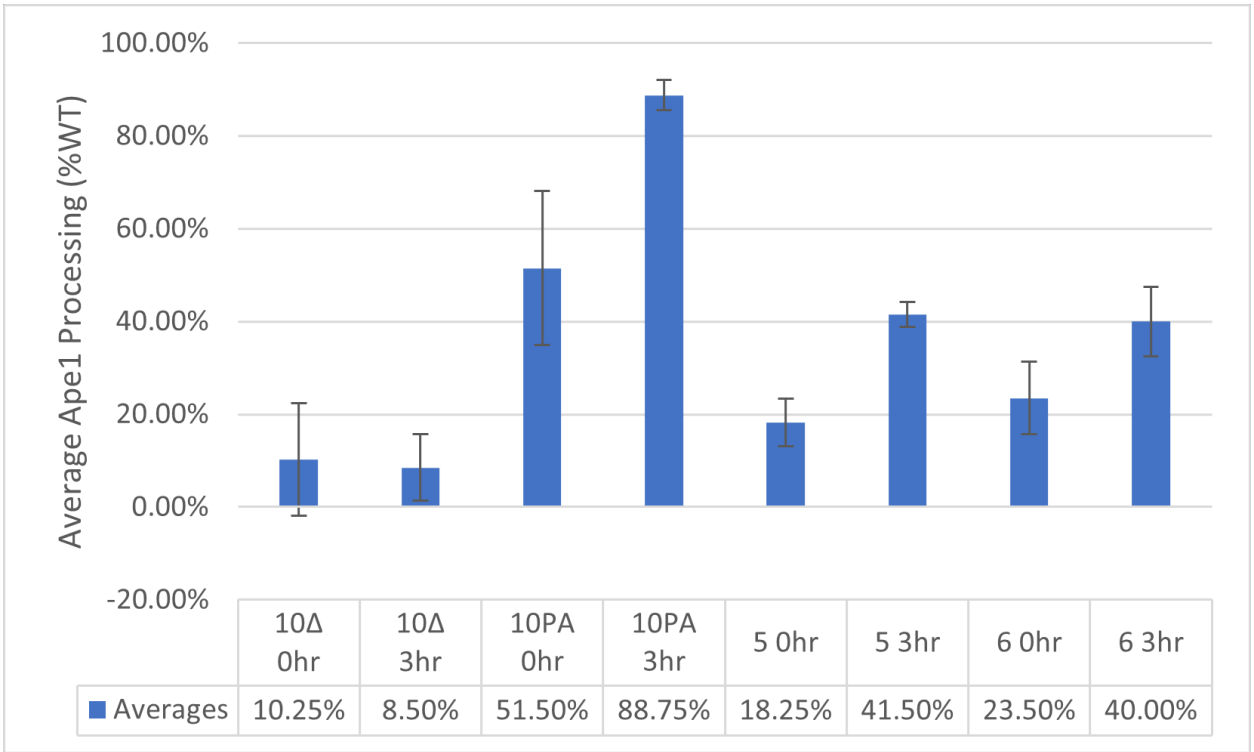

C.

Figure 5: Ape1 processing results suggest that atg10-PA H131A Y73Q Clones 5 and 6 have reduced autophagic function when compared to Atg10-PA. Clones 5 and 6 are two identical clones of pRS406 atg10-PA H131A Y73Q. (A) WLY176 *atg10Δ*, which lacks the *ATG10* gene,

was the negative control and WLY176 Atg10PA was the positive control. The 0 hour samples were harvested immediately after growing to log phase in YPD, whereas the 3 hour samples were starved in SD-N (a nitrogen starvation medium) for 3 hours. Ape1 processing and Atg10-PA levels were analyzed by immunoblotting with anti-Ape1 and PAP antibodies, respectively, with anti-Pgk1 antibodies serving as a loading control. Cells with Atg10-PA were able to cleave the pre-Ape1 to form mature Ape1(mApe1). (B) The PAP signal was quantified using ImageJ. The PAP over total Pgk1 was expressed as a percent. N=3 independent replicates. (C) Levels of pre-Ape1 and mApe1 were quantified using ImageJ, then mApe1 over the total Ape1 was expressed as a percent. N=4 independent replicates. The error bars in both B and C represent the 95% Confidence Interval meaning that we are 95% certain this range contains the average.

Western blots for Pgk1, PAP, and Ape1 were carried out. Pgk1 was used as a loading control and was therefore present in all lanes, while PAP was used to verify the PA tag on Atg10 and was therefore present in all the samples which have the PA tag, which includes the Wild Type and the mutants (Figure 5A). Additionally, because PA is tagged to Atg10 it is a measure of how much Atg10 was present in each lane (Figure 5B). The mutants had a more intense PAP band, which was a result of them having higher levels of Atg10; this is consistent with past results in our lab as well as other labs (Nadia 2022, Yamaguchi *et al.* 2012). Ape1 processing is actually a selective autophagy process and measures the overall autophagic activity; it is a zymogen (inactive protease) in the cytosol and is activated in the vacuole after being cut by another protease (Noda and Klionsky 2008). Ape1 is found throughout the cytoplasm of the cell, so when autophagy takes place and the Ape1 cargo is selectively transported to the vacuole, it will be cleaved into the mature form. The increase in non-selective autophagy induced by nitrogen starvation stimulates selective autophagy which makes this a good tool for verifying overall autophagic activity (Noda and Klionsky 2008). Because we know the vacuole is the end target of autophagy, we can say that if the Ape1 protease gets into the vacuole then we have evidence of autophagy and the cascade from Atg10 to Atg8 was successful. On the western blot this translates to different (lower) band sizes because cleaved Ape1 is smaller. As a result, we

saw a pattern where the 0hr samples had a higher band (preApe1, approximately 55kD) compared to the 3hr samples where the Ape1 had been cleaved (mApe1, approximately 48 kD) (Figure 5A). However, the *atg10Δ* sample was lacking the *ATG10* gene and autophagy was halted almost completely, which explains the absence of a lower band even in the 3hr sample. The difference in intensity of the lower bands was also noticeable in the Atg10 mutant clones 5 and 6, suggesting that the WT still has the most efficient autophagic function, while the mutants have reduced function, which is the goal of our double mutant.

These differences in intensity were measured in ImageJ and quantified (Figure 5B), the negative control *atg10Δ* 3hr measured 9%, while the positive control Atg10-PA 3hr measured 89%, which is expected as its *ATG10* gene should be fully functional. Clones 5 and 6 3hr of pRS406 Atg10-PA H131A Y73Q measured 42% and 40% respectively, thus verifying a reduction in Ape1 processing.

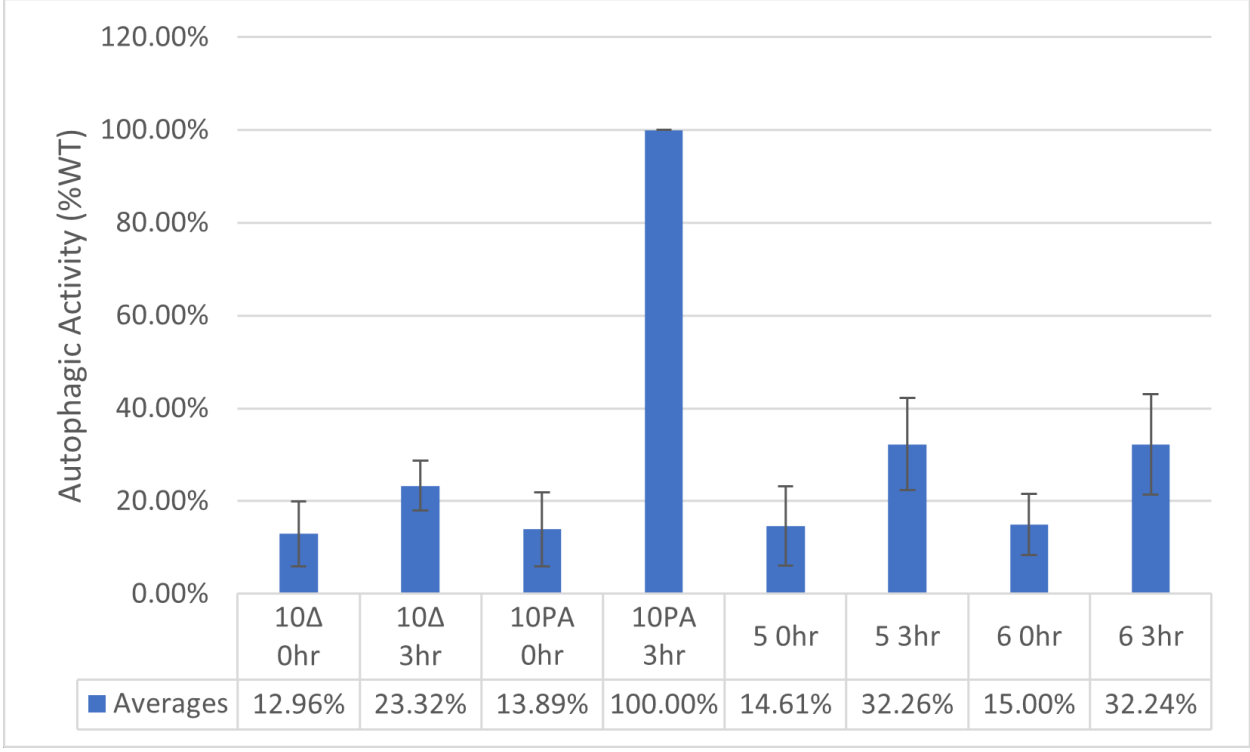

Figure 6: The Pho8Δ60 assay verifies the defect of overall autophagic activity in our double mutant when compared to wild type. All strains were grown in rich medium in log phase and then starved in nitrogen-starvation medium for 3 hours. Autophagic activity was quantified by the pho8Δ60 assay, with each replicate independently normalized to the Atg10-PA 3hr starved cells. The knockout strain *atg10Δ* (10Δ) was the negative control and PA tagged Atg10 (10PA) were the positive controls. N= 4 independent replicates for all samples except Atg10PA 3hr (N=3). The error bars represent the 95% Confidence Interval.

Following the Ape1 processing results, a Pho8△60 enzymatic assay was performed to compare our mutant strains to the wild type. This assay allows us to "quantify the autophagic flow in yeast" (Noda and Klionsky, 2008). Pho8 is a vacuolar enzyme that is brought to the vacuole by the secretory pathway. We used a genetically modified version, pho8△60, which is missing the signal that allows it to be anchored to the membrane, meaning it just stays within the cytosol. As a result of non-selective autophagy the pho8△60 ends up in the vacuole where the C-terminal autoinhibitory domain is removed and it is activated. We can measure the amount activated by breaking open the cells and incubating them with a clear substrate; the phosphatase activity from active pho8△60 changes the substrate into a yellow-colored compound. As a result, the activity of the phosphatase correlates directly with the amount of cytosol delivered to the vacuole via autophagy. The 10PA wild type showed the most activity, while the mutants had much more reduced autophagic activity, suggesting that the mutations, Y73Q and H131A, were successful in reducing the activity of atg10 and therefore autophagic function as a whole (Figure 6).

SECTION 5: DISCUSSION

We know from previous studies that Atg7 activates both the Atg10 and Atg3 pathways. The Atg10 pathway goes on to conjugate Atg12-5-16, which upregulates Atg3, ultimately allowing for Atg8-PE lipidation (Martens and Fracchiolla 2020). A previous study also determined that

Atg7 affects autophagosome size and number, while Atg8 affects primarily autophagosome size (Cawthon et al. 2018). Given this information, we hypothesize that Atg3 and Atg10 also affect either size, number, or both. This work focuses on Atg10.

As described in the results section, we now have a double mutant (H131A and Y73Q) of Atg10 that has a greater reduction in function than the previous H131A and Y73Q single mutations. This was verified empirically with western blots as well as the ALP assay. It is important to note that this reduction in autophagy in the double mutant is not synonymous with the elimination of autophagy; 30-40% residual autophagic activity remains.

Previous studies by Yamaguchi et al. have shown that these mutations in atg10 cause a reduction in the conjugation of the atg12-15-16 complex, a step which is required for the ultimate Atg8-PE lipidation (2012). As a result, some additional testing of the mutant will likely be required to verify reduction in function in terms of other conjugations in the autophagic cascade, like the complex just mentioned (Figure 3). Additionally, a western blot will be performed measuring the Atg 10 double mutants effect on the conjugation of Atg8 to PE (phosphatidylethanolamine), a molecule located in the lipid membrane of the autophagosome or phagophore (Nair *et al.* 2012).

In previous experiments in the lab where the single mutants were used and the matureApe1 had only a 10% reduction when compared to Atg10-PA, the Atg8-PE conjugation was not significantly affected (Silvia 2022). With the double mutant giving a much lower percent of autophagic activity in both Ape1 and the ALP assay we would expect to see a greater reduction in these conjugation systems.

In upcoming experiments, once several suitable mutants have been generated and verified, we will be able to take cross-sectional images of the yeast cells in starved and unstarved

conditions, using a Transmission Electron Microscope at the at the U of M MIL (Microscopy and Image Analysis Laboratory). Once these steps have been completed, Adobe Photoshop will be used to outline the autophagic bodies, and the outlines can then be utilized for the estimations of body size and number. These estimations will be made from the raw measurements of the autophagic body crossections using mathematical equations outlined by Backues et al. (2014). This will allow us to quantify both the size and number of the autophagosomes in response to the reduction in function of the Atg10 double mutant we generated, ultimately allowing us to determine the effect Atg10 has in the autophagic cascade.

SECTION 6: REFERENCES

Backues, S. K., Chen, D., Ruan, J., Xie, Z., & Klionsky, D. J. (2014). Estimating the size and number of autophagic bodies by electron microscopy. Autophagy, 10(1), 155–164. https://doi.org/10.4161/auto.26856

Cawthon, H., Chakraborty, R., Roberts, J. R., & Backues, S. K. (2018). Control of autophagosome size and number by Atg7. Biochemical and Biophysical Research Communications, 503(2), 651–656. https://doi.org/10.1016/j.bbrc.2018.06.056

Choi, A. M. K., Ryter, S. W., & Levine, B. (2013). Autophagy in Human Health and Disease. New England Journal of Medicine, 368(7), 651–662. https://doi.org/10.1056/NEJMra1205406

Davis, M. W., & Jorgensen, E. M. (2022). ApE, A Plasmid Editor: A Freely Available DNA Manipulation and Visualization Program. Frontiers in Bioinformatics, 2. https://www.frontiersin.org/articles/10.3389/fbinf.2022.818619

Gietz, R. D., & Schiestl, R. H. (2007). High-efficiency yeast transformation using the LiAc/SS carrier DNA/PEG method. Nature Protocols, 2(1), 31–34. https://doi.org/10.1038/nprot.2007.13

Kanki, T., Wang, K., Baba, M., Bartholomew, C. R., Lynch-Day, M. A., Du, Z., Geng, J., Mao, K., Yang, Z., Yen, W.-L., & Klionsky, D. J. (2009). A Genomic Screen for Yeast Mutants Defective in Selective Mitochondria Autophagy. Molecular Biology of the Cell, 20(22), 4730–4738. https://doi.org/10.1091/mbc.E09-03-0225

Longtine, M. S., Mckenzie III, A., Demarini, D. J., Shah, N. G., Wach, A., Brachat, A., Philippsen, P., & Pringle, J. R. (1998). Additional modules for versatile and economical PCR-based gene deletion and modification in Saccharomyces cerevisiae. Yeast, 14(10), 953–961. https://doi.org/10.1002/(SICI)1097-0061(199807)14:10<953::AID-YEA293>3.0.CO;2-U

Martens, S., & Fracchiolla, D. (2020). Activation and targeting of ATG8 protein lipidation. Cell Discovery, 6, 23. https://doi.org/10.1038/s41421-020-0155-1

Matoba, K., & Noda, N. N. (2021). Structural catalog of core Atg proteins opens new era of autophagy research. Journal of Biochemistry, 169(5), 517–525. https://doi.org/10.1093/jb/mvab017

Nair, U., Yen, W.-L., Mari, M., Cao, Y., Xie, Z., Baba, M., Reggiori, F., & Klionsky, D. J. (2012). A role for Atg8–PE deconjugation in autophagosome biogenesis. Autophagy, 8(5), 780–793. https://doi.org/10.4161/auto.19385

Noda, T., & Klionsky, D. J. (2008). The quantitative Pho8Delta60 assay of nonspecific autophagy. Methods in Enzymology, 451, 33–42. https://doi.org/10.1016/S0076-6879(08)03203-5

Reggiori, F., & Klionsky, D. J. (2002). Autophagy in the Eukaryotic Cell. Eukaryotic Cell, 1(1), 11–21. https://doi.org/10.1128/EC.01.1.11-21.2002

Reggiori, F., & Klionsky, D. J. (2013). Autophagic processes in yeast: mechanism, machinery and regulation. Genetics, 194(2), 341–361. https://doi.org/10.1534/genetics.112.149013

Roberts, J. (n.d.). THE EFFECTS OF POINT MUTATIONS IN ATG3 ON AUTOPHAGIC ACTIVITY.

Silvia, N. (n.d.).

Xie, Z., & Klionsky, D. J. (2007). Autophagosome formation: core machinery and adaptations. Nature Cell Biology, 9(10), 1102–1109. https://doi.org/10.1038/ncb1007-1102

Yamaguchi, M., Noda, N. N., Yamamoto, H., Shima, T., Kumeta, H., Kobashigawa, Y., Akada, R., Ohsumi, Y., & Inagaki, F. (2012). Structural insights into Atg10-mediated formation of the autophagy-essential Atg12-Atg5 conjugate. Structure (London, England: 1993), 20(7), 1244–1254. https://doi.org/10.1016/j.str.2012.04.018

Yamasaki, A., & Noda, N. N. (2017). Structural Biology of the Cvt Pathway. Journal of Molecular Biology, 429(4), 531–542. https://doi.org/10.1016/j.jmb.2017.01.003

Frontiers | ApE, A Plasmid Editor: A Freely Available DNA Manipulation and Visualization Program. (n.d.). Retrieved November 9, 2022, from https://www.frontiersin.org/articles/10.3389/fbinf.2022.818619/full